Structural and optical properties of Pd²⁺-doped mesoporous TiO₂ thin films prepared by sol-gel templating technique

B. YARMAND [*], S. K. SADRNEZHAAD [a]

Department of New Materials, Materials and Energy Research Center, Karaj, Iran
[a] *Department of Material Science and Engineering, Sharif University of Technology, Tehran, Iran*

Pd²⁺-doped TiO₂ thin films with mesoporous structure were produced on quartz substrate by sol-gel dip coating. The structural, morphological and optical properties of the film were characterized by X-ray diffraction (XRD), Brunauer–Emmett–Teller (BET), transmission electron microscopy (TEM), atomic force microscopy (AFM) and UV/vis transmittance spectroscopy. By increasing the Pd²⁺ concentration from 0 to 6 mol%, the crystallites appeared solely as the anatase phase and their average sizes decreased from 10.5 to 7.1 nm. Addition of Pd²⁺ also resulted in increasing of the specific surface area and decreasing of the pore size of the layer. The transmittance of the films decreased in the visible light region and the absorption edges shifted to the longer wavelengths by increasing of the Pd²⁺ doped concentration. Optical band-gaps of the undoped and 6 mol% Pd²⁺-doped films were 3.52 and 3.31 eV, respectively. The refractive index of the films decreased from 1.83 to 1.71 and their porosity increased from 56.3 to 63.7% by increasing of the Pd²⁺ doping concentration from 0 to 6 mol%.

1. Introduction

TiO₂ thin films with mesoporous structure have extensive applications in photocatalysis [1, 2], dye-sensitized solar cells [3, 4], sensors [5], rechargeable lithium batteries [6, 7] and many other applications due to their easy synthesis, great chemical stability, low cost, extraordinary optical and electrical properties and versatile other capabilities [8, 9]. Extensive application of TiO₂ in solar cells is bound to two limitations:

• Wide band-gap of TiO₂ being excitable with ultraviolet radiations having wavelengths below 387 nm. These waves only make a small part of solar spectrum (about 4 %). The return of using solar radiation will then be very low [10, 11].

• Large recombination rate of photo-excited electron-hole pairs causing low percentage usable charges [12].

An appropriate simple solution of these limitations is dopant usage. Quantum sized TiO₂ doping with various transitional metal ions improves interfacial electron transfer rate, recombination rate, charge carrier generation and photo reactivity [13-15].

Various deposition techniques such as electron beam evaporation [16], metal organic chemical vapor deposition (MOCVD) [17], pulsed laser deposition [18], reactive sputtering technique [19], spray pyrolysis [20], hydrothermal process [21] and sol-gel methods [22] have been used for production of TiO₂ thin films.

Besides the above methods, sol-gel technique can be considered as the most influential technique for preparation of the mesoporous thin layers. It can provide good homogeneity, uniform composition and large specific areas via mild processing conditions [23, 24]. A combination of the evaporation-induced self-assembly (EISA) using structure-directing polymer (template) with complexation of molecular inorganic species in precursor can be used to prepare the mesoporous films through sol-gel process [25].

Although the influence of doped transitional metal ions like Fe, Cd, Cr, Nb, Co, Ni and Sn on the thin film TiO₂ is almost known, there is not sufficient information yet made available on the effect of Pd²⁺ on properties of mesoporous TiO₂ thin layers [26-30]. Because of the ionic radius differences imposed on the Ti⁴⁺, it is expected that Pd²⁺ doping causes remarkable change on characteristics of the TiO₂ films. This paper indicates the recently obtained findings about the influence of the Pd²⁺-doping process on structural, morphological and optical properties of the mesoporous TiO₂ thin layers produced by the sol-gel templating process.

2. Experimental

2.1. Materials and chemicals

Titanium tetraisopropoxide [Ti (O·i-C₃H₇)₄] 98% (Merck) was used as precursor, hydrochloric acid (HCl) 32% (Merck) was utilized as catalyst, non-ionic triblock copolymer surfactant Pluronic P123 [poly-(ethylene oxide)

poly-(propylene oxide) poly-(ethylene oxide) EO_{20}–PO_{70}–EO_{20}] (Aldrich) was employed as template, ethanol (C_2H_5OH) 99.9% (Merck) was used as solvent and Palladium chloride ($PdCl_2$) 59%Pd (Merck) was utilized as dopant. All chemicals were used in the as-received form in the experiments. Quartz slide substrates were applied for deposition of the thin layers.

2.2. Production of mesoporous Pd²⁺-doped TiO₂ thin film

Mesoporous TiO₂ thin films were prepared by self-assembly of the P123 triblock copolymer surfactant in sol-gel solution. Room temperature stirring of 5 g Ti (O·i-C_3H_7)₄ with 3.2 g HCl for 10 min resulted in hydrolysis to occur. The hydrolyzed sol was mixed with 1 g P123 surfactant being dissolved in 21 g ethanol while being stirred for 10 min at the room temperature. Different amounts of palladium chloride were finally added to the solution. The molar ratios of Pd²⁺ to Ti⁴⁺ were 0, 0.02, 0.04 and 0.06. Quartz substrates subsequently received the required coatings by repeated dipping and withdrawing procedure. The rate of coating was 60 mm/min. The films were then aged for 24 h under controlled humidity of 65-75 % at temperature of 10 °C. The samples were finally annealed under air for 1 h at 500°C inside a tube furnace which was heated up at the heating rate of 1.0 °C/min. Before coating, the quartz substrate having dimensions of $2.5 \times 1.25 \times 0.2$ cm³ were degreased, thoroughly cleaned and dried in an oven at 120°C for 30 min.

2.3. Product characterization

Phase identification and crystallite size determination were achieved by X-ray diffractometer (Philips, PW3710) using Cu-K$_\alpha$ radiation and Ni filter operating at 40 kV and 30 mA. The scanning range was from 20 to 80 ° with a scanning rate of 0.25 °min⁻¹. The specific surface area of the films was determined through nitrogen adsorption/desorption isotherms (BELSORP 2). The Brunauer–Emmet–Teller (BET) specific surface area was calculated from the linear part of the BET plot (P/P₀ = 0.05 – 0.35). The pore size distribution plots were obtained by using the Barret–Joyner–Halenda (BJH) model. The surface relief and morphology of the films were observed using atomic force microscopy (Auto probe, CP) and transmission electron microscopy (Philips, CM200 FEG), respectively. The optical transmittance spectra of the films were recorded using a UV/vis spectrophotometer (Perkin Elmer, Lambda 25) with a scanning rate of 60nm/min in the wavelength range of 200 – 800 nm.

3. Results and discussion

3.1. Structural studies

The wide-angle XRD patterns of the powders scraped from the Pd²⁺-doped mesoporous TiO₂ thin films of various concentrations are shown in Fig. 1. Phase identification indicates that all samples have anatase phase. No peaks confirming the presence of the palladium oxide (Pd_xTiO_y) or other compounds like carbon-containing impurity phases are observable in the figure. It can be concluded that Pd²⁺ ions may occupy the interstices or ordinary lattice sites of the TiO₂ layer when forming a palladium-titanium solid solution [31]. The strongest peaks observed for anatase phase at different doping concentrations are (101) 2θ=25.3°, (004) 2θ=37.8° and (200) 2θ=48.0° [32]. By increasing Pd²⁺-doping concentration from 0 to 6 mol%, the intensity of the anatase peaks slightly decreases and the width of (101) plane diffraction peak becomes boarder. This corresponds to the crystallite weakening event.
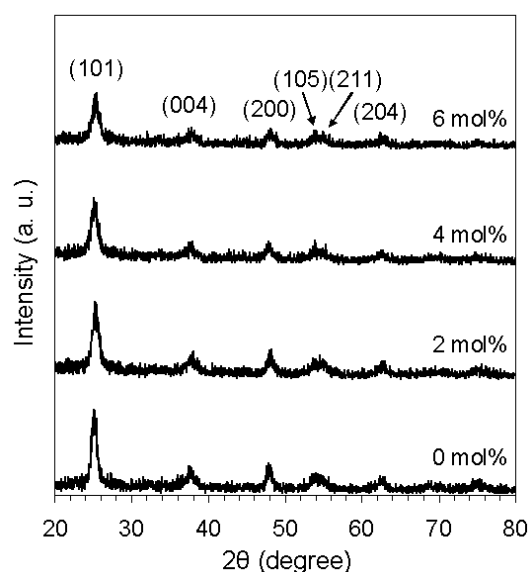
Fig. 1. Wide-angle XRD patterns of Pd²⁺-doped mesoporous TiO₂ samples of various concentrations given in the figure.

The average crystallite size of the anatase phase in mesoporous TiO₂ thin films can be calculated from the XRD data by using Scherrer equation [33]:

$$D = \frac{k\lambda}{B\cos\theta}$$

where D is the average crystallite size, λ is the applied X-ray wavelength (λ=1.5406 Å), k=0.90 which is a constant, θ is the diffraction angle in degree and B is the full width at half maximum (FWHM) of the diffraction peak observed in radians. Fig. 2 shows the effect of Pd²⁺-doping concentration on anatase crystallite size of the mesoporous TiO₂ thin films. The anatase crystallite size of the undoped sample is 10.5 nm and decreases to 7.1 nm by increasing Pd²⁺-doping concentration to 6 mol%. Increasing Pd²⁺-doping concentration increases the number of located Pd²⁺ ions in TiO₂ lattice. The presence of these ions inhibits the

growth of anatase nanocrystals. It is possible that exceeding increase of located Pd^{2+} ions in TiO_2 lattice delays phase transition from amorphous to anatase phase [30].
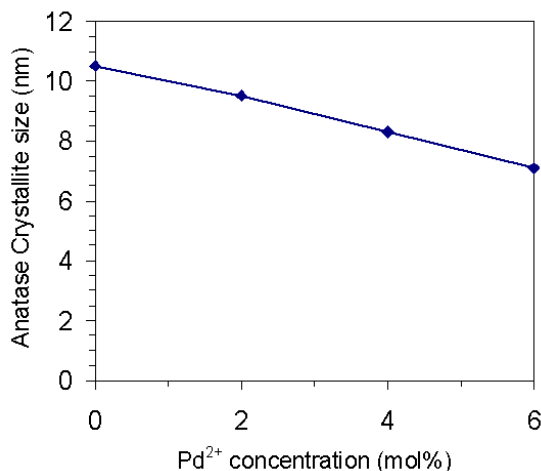
Fig. 2. Variation of anatase crystallite size with Pd^{2+}-doping concentration.

3.2. Specific surface area

The N_2 adsorption/desorption isotherms and Barrett-Joyner-Halenda (BJH) analysis of adsorption branches of powders scraped from the mesoporous TiO_2 thin films doped with various concentration of Pd^{2+} are shown in Fig. 3. All isotherms have stepwise manner and show a type-4 curve that proves the TiO_2 thin films having mesoporous structure [34]. The BJH analysis shows that all films have narrow pore size distribution in the range of 1.6 to 10.5nm and the average diameter of their pores is from 4.52 to 6.18 nm. The narrow pore size distribution curves indicating mesoporous TiO_2 thin films having uniform pore channels. Variation of the specific surface area and pore size of the mesoporous TiO_2 thin films doped with Pd^{2+} are shown in Table 1. It can be seen that by increasing Pd^{2+}-doping concentration, the specific surface area increases, while the pore diameter decreases. These changes in surface and pore properties of the mesoporous TiO_2 thin films might be the result of the inhibition of the crystallites from growth and leaving behind of the small pores. According to the XRD results, increasing Pd^{2+}-doping concentration inhibits the growth of the anatase nanocrystals resulting in smaller nanocrystals having larger specific areas. Inhibition of anatase nanocrystals from growth prevents elimination of the fine pores. The result is appearance of many small pores with their average total volume increase.
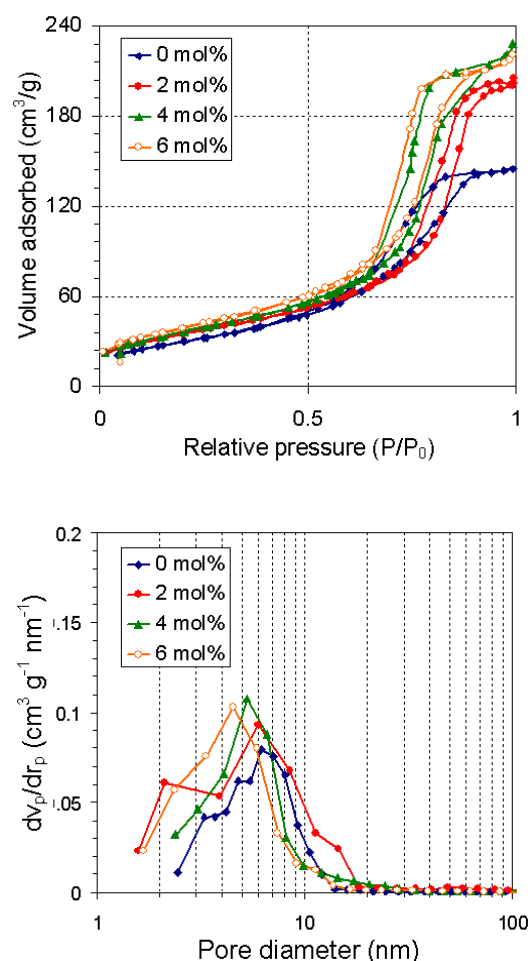
Fig. 3. Effect of Pd^{2+} concentration on N_2 adsorption/desorption isotherms and Barret-Joyner-Halenda (BJH) pore size distribution for adsorption branches of the mesoporous TiO_2 thin films produced in this research.

3.3. Morphology investigation

Fig. 4 shows AFM images of the undoped and 6 mol% Pd^{2+}-doped mesoporous TiO_2 thin films. Both films illustrate uniform hill-valley like morphologies with the same roughness. It is observed that the addition of up to 6 mol% Pd^{2+} ion dopant have no effect on topography of the mesoporous TiO_2 thin layer. Fig. 5 shows TEM images of mesoporous TiO_2 doped with 6 mol% Pd^{2+} thin filmed on quartz substrate. The film is seen to have homogeneous porous structure. It can be concluded that the anatase nanocrystals connect to each other to form a framework consisting of mesopores. The thickness of the film is another crucial factor measured by SEM cross-sectional image. The average thickness of the films with single-cycle dip coating practice is estimated to be about 120 nm.

Table 1. Specific surface area and pore size of mesoporous TiO₂ thin films having various Pd²⁺-doping concentrations.

Doping concentration (mol%)	Specific surface area (m²/g) [by BET]	Mean pore diameter (nm) [by BET]	Average pore diameter (nm) [by BJH, adsorption]	Average pore diameter (nm) [by BJH, desorption]
0	108.91	8.21	6.18	6.18
2	125.87	7.55	5.97	5.10
4	131.77	6.62	5.22	4.06
6	140.63	5.64	4.52	3.05

0 mol% (rms = 2.034 nm)

6 mol% (rms = 2.115 nm)
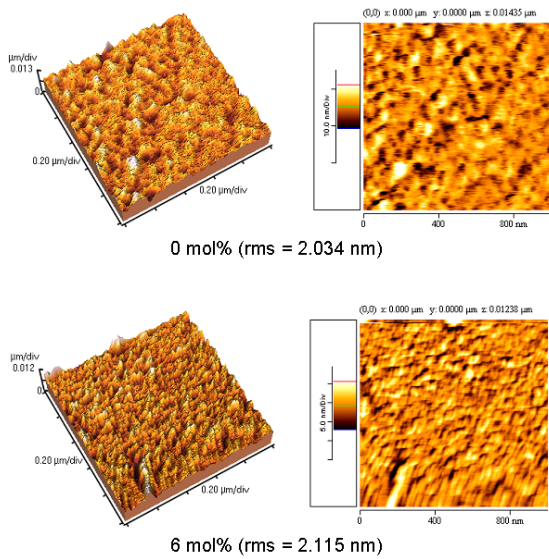
Fig. 4. AFM images of undoped and 6 mol% Pd²⁺-doped mesoporous TiO₂ thin films.

Fig. 5. TEM images of the 6 mol% Pd²⁺-doped mesoporous TiO₂ thin film.
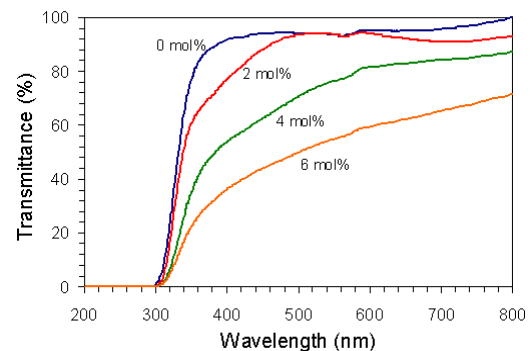
Fig. 6. Optical transmittance spectra of the mesoporous TiO₂ thin films doped with various concentration of Pd²⁺.

3.4. Optical characterization

The ultraviolet-visible (UV-vis) transmittance spectra of mesoporous TiO₂ thin films doped with various concentration of Pd²⁺ in the wavelength range of 200-800 nm are shown in Fig. 6. All films exhibit good transmittance in the visible region and a sharp fall in the UV region which corresponds to the absorption of light caused by the excitation of electrons from the valence band to the conduction band of the TiO₂ semiconductor. It can be observed that by increasing Pd²⁺-doping concentration, the samples show a stronger absorption in the visible region and the absorption edges shift to longer wavelengths. The red shift of the absorption edges is a result of charge transfer transition between the palladium d electrons and the valance and conduction bands of TiO₂ thin layers [35].

The optical band-gap (Eg) in a semiconductor is determined by Tauc's equation [36]:

$$\alpha = \frac{k\left(h\upsilon - E_g\right)^n}{h\upsilon}$$

where α is optical absorption coefficient, k is a constant, $h\upsilon$ is the photon energy (eV) and n may have different values of 1/2, 2, 3/2 or 3 for allowed direct and indirect and forbidden direct and indirect transitions, respectively [37]. The optical band-gap is estimated by extrapolating the straight-line portion of the $(\alpha h\upsilon)^{1/2}$ vs. $h\upsilon$ plot (Fig. 7). The intercept on the energy axis has been noted down for different Pd²⁺-doping concentration. Fig. 8 shows the

change in optical band-gap with Pd^{2+}-doping concentration. The band-gap of the undoped film is 3.52 eV and it gradually decreases to 3.31 eV after doping with 6 mol% of Pd^{2+}. The decrease in the optical band-gap of the mesoporous TiO_2 thin films with Pd^{2+}-doping concentration might be a result of the change in characteristics of TiO_2 films. Due to presence of Pd^{2+} ions in TiO_2 lattice, the palladium d orbital admix with TiO_2 and create new intermediate energy levels inside TiO_2 band-gap. As a result of these, charge transfer transition becomes narrower and the Fermi level of TiO_2 films decreases. Therefore, the excitation of dopped films occurs with lower energy radiation [38]. The observed values are higher than the band-gap of both bulk and thin film TiO_2. The larger band-gap of the film in comparison to their bulk values is contributed to the lattice deformation by an axial strain [39]. The higher band-gap observed in our case can be due to the quantum size effects arising from the small size of TiO_2 nanocrystallites present in the mesoporous thin layer [40].
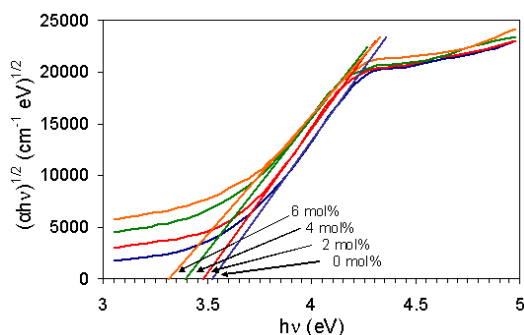
Fig. 7. The plot of $(\alpha h\nu)^{1/2}$ vs. $h\nu$ for mesoporous TiO_2 thin films doped with Pd^{2+} at different concentrations.
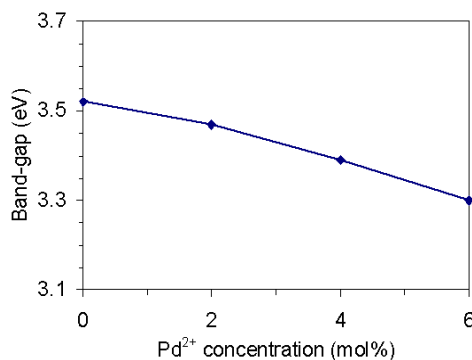
Fig. 8. Optical band-gap estimated for mesoporous TiO_2 thin films doped with Pd^{2+} at different concentrations.

The refractive index (n) of the transparent films is determined using the Swanepoel Envelope method [41]. Maximum and minimum transmittance values (T_{max} and T_{min}) are recorded from optical transmittance spectra shown in Fig. 6. The refractive index can be calculated from the above values by applying the following relation [42]:

$$n = \sqrt{N + \sqrt{N^2 - n_0^2 n_1^2}}$$

where

$$N = \frac{n_0^2 + n_1^2}{2} + 2n_0 n_1 \frac{T_{max} - T_{min}}{T_{max} T_{min}}$$

n_0 and n_1 are the refractive indices of air and substrate, respectively, T_{max} is the maximum envelope and T_{min} is the minimum envelope. The porosity of the films is calculated using the following equation [43]:

$$Porosity = \left[1 - \left(\frac{n^2 - 1}{n_d^2 - 1}\right)\right] \times 100$$

where n_d is the refractive index of the pore-free TiO_2. It is seen that the porosity of the prepared thin film is quite higher than that of the bulk anatase TiO_2 phase. Fig. 9 shows the variation of the refractive index at 550-nm and the porosity of the mesoporous TiO_2 thin films doped with various concentrations of Pd^{2+}. The values of the refractive index are lower than that of the bulk TiO_2 (2.54 for the anatase phase) probably due to the narrow size of the grains [44]. An increase in Pd^{2+}-doping concentration from 0 to 6 mol% results in decreasing of the refractive index from 1.83 to 1.71 and increasing of the porosity from 56.3 to 63.7%. The decrease of the film refractive index by Pd^{2+}-doping concentration can be attributed to the crystallite weakening and film porosity increasing because of refractive index dependence on factors such as crystallinity, electronic structures, density and defects [45].
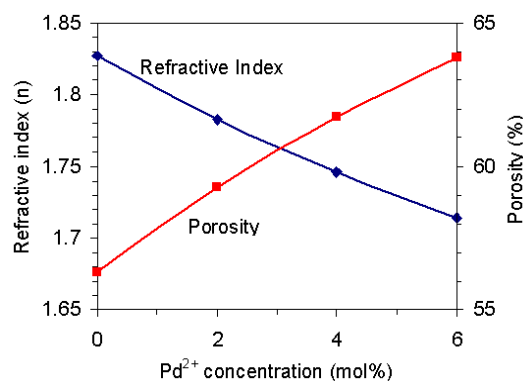
Fig. 9. Variation of the refractive index at 550-nm wavelength and porosity of the mesoporous TiO_2 thin film doped with Pd^{2+} at different concentrations.

4. Conclusion

Mesoporous TiO_2 thin films doped with Pd^{2+} ions at different concentrations were successfully prepared on quartz substrate by sol-gel dip-coating templating technique. The effects of Pd^{2+}-doped concentration on structural, morphological and optical properties of the films were determined. Phase identification showed that all films had anatase phase and the crystallite size

decreased from 10.5 to 7.1 nm by increasing of the Pd^{2+}-doping concentration from 0 to 6 mol %. The specific surface area of the undoped film was 108.91 m^2/g and increased to 140.63 m^2/g at 6 mol% of Pd^{2+}-doping concentration. The mean squared value of the film roughnesses was the same. As the Pd^{2+}-doping concentration increased, the transmittance of the films decreased in the visible region and the absorption edges shifted to the longer wavelengths. The estimated optical band-gap of the films decreased from 3.52 to 3.31eV by increasing Pd^{2+}-doping concentration from 0 to 6 mol%. The refractive index of the films decreased from 1.83 to 1.71 with enhancement of the Pd^{2+}-doping concentration from 0 to 6 mol% and increasing of the porosity from 56.3 to 63.7%.

References

[1] N. Venkatachalam, M. Palanichamy, V. Murugesan, Mater. Chem. Phys. **104**, 454 (2007).

[2] S. Z. Chu, S. Inoue, K. Wada, D. Li, H. Haneda, S. Awatsu, J. Phys. Chem. B **107**, 6586 (2003).

[3] A. C. Arango, L. R. Johnson, V.N. Bliznyuk, Z. Schlesinger, S. A. Carter, Adv. Mater. **12**, 1689 (2000).

[4] A. C. Arango, S. A. Carter, P. J. Brock, Appl. Phys. Lett. **74**, 1698 (1999).

[5] O. K. Varghese, D. W. Gong, M. Paulose, K. G. Ong, E. C. Dickey, C. A. Grimes, Adv. Mater. **15**, 624 (2003).

[6] L. Kavan, J. Rathousky, M. Grätzel, V. Shklover, A. Zukal, J. Phys. Chem. B **104**, 1012 (2000).

[7] O. Wilhelm, S. E. Pratsinis, E. de Chambrier, M. Crouzet, I. Exnar, J. Power Sources **134**, 197 (2004).

[8] G. K. Mor, O. K. Varghese, M. Paulose, K. Shankar, C. A. Grimes, Sol. Energy Mater. Sol. Cells **90**, 2011 (2006).

[9] R. Zhang, L. Ga, Q. Zhang, Chemosphere **54**, 405 (2004).

[10] X. T. Hong, Z. P. Wang, W. M. Cai, F. Lu, J. Zhang, Y. Z. Yang, N. Ma, Y. J. Liu, Chem. Mater. **17**, 1548 (2005).

[11] J. C. Yu, J. G. Yu, W. K. Ho, Z. T. Jiang, L. Z. Zhang, Chem. Mater. 14, 3808 (2002).

[12] T. Tong, J. Zhang, B. Tian, F. Chen, D. He, J Hazard Mater **155**, 572 (2008).

[13] J. Soria, J. C. Conesa, V. Augugliaro, L. Palmisano, M. Schiavello, A. Sclafani, J. Phys. Chem. **95**, 274 (1991).

[14] W. Choi, A. Termin, M. R. Hoffmann, J. Phys. Chem. **98**, 13669 (1994).

[15] J. Moon, H. Takagi, Y. Fujishiro, M. Awano, J. Mater. Sci. **36**, 949 (2001).

[16] D. Bhattacharyya, N. K. Sahoo, S. Thakur, N. C. Das, Thin Solid Films **360**, 96 (2000).

[17] X. W. Zhang, M. H. Zhou, L. C. Lei, Catal Commun **7**, 427 (2006).

[18] E. Gyorgy, G. Socol, E. Axente, I. N. Mihailescu, C. Ducu, S. Ciuca, Appl. Surf. Sci. **247**, 429 (2005).

[19] D. Mardare, V. Nica, C.M. Teodorescu, D. Macovei, Surface Science **601**, 4479 (2007).

[20] I. Oja, A. Mere, M. Krunks, R. Nisumaa, C. H. Solterbeck, M. Es-Souni, Thin Solid Films **515**, 674 (2006).

[21] S. Kambe, K. Murakoshi, I. Kitamura, Y. Wada, S. Yanagida, H. Kominami, Y. Kera, Sol. Energy Mater. Sol. Cells **61**, 427 (2000).

[22] U. Cernigoj, U. L. Stangar, P. Trebxe, U. O. Kraxovec, S. Gross, Thin Solid Films **495**, 327 (2006).

[23] H. Yun, K. Miyazawa, I. Honma, H. Zhou, M. Kuwabara, Mat. Sci. and Eng. C **23**, 487 (2003).

[24] K. Liu, M. Zhang, K. Shi, H. Fu, Materials Letters **59**, 3308 (2005).

[25] C. J. Brinker, Y. F. Lu, A. Sellinger, H. Y. Fan, Adv. Mater. **11**, 579 (1999).

[26] F. E. Ghodsi, F. Z. Tepehan, G. G. Tepehan, Sol. Energy Mater. Sol. Cell. **68**, 355 (2001).

[27] A. Rampaul, I. P. Parkin, S. A. O'Neill, J. Desouza, A. Mills, N. Elliott, Polyhedron **22**, 35 (2003).

[28] F. Gracia, J. P. Holgadu, L. Contreras, T. Girardeau, A. R. Gonzalez-Elipe, Thin Solid Films **429**, 84 (2003).

[29] J. Zhu, W. Zheng, B. He, J. Zhang, M. Anpo, J. Molec. Catal. A: Chem. **216**, 35 (2004).

[30] M. Zhou, J. Yu, B. Cheng, H. Yu, Mater. Chem. Phys. **93**, 159 (2005).

[31] C. Y. Wang, C. Bottcher, D. W. Bahnemann, J. K. Dohrmann, J. Mater. Chem. **13**, 2322 (2003).

[32] JCPDS PDF 01-071-1166

[33] B. D. Cullity, Elements of X-ray diffraction, Wesley Publishing Company Inc, London (1978).

[34] N. Wark, J. Tschirch, O. Bartels, D. Bahnemann, J. Rathousky, Micropor. Mesopor. Mater. **84**, 247 (2005).

[35] D. H. Kim, H. S. Homg, S. J. Kim, J. S. Song, K. S. Lee, J. Alloys Compounds **375**, 259 (2004).

[36] M. Sreemany, S. Sen, Materials Chemistry and Physics **83**, 169 (2004).

[37] D. Bhattacharyya, S. Chaudhuri, A. K. Pal, Vacuum **43**, 313 (1992).

[38] M. Radecka, P. Pasierb, K. Zakrzewska, M. Rekas, Solid State Ionics **119**, 43 (1999).

[39] H. C. Ong, A. X. E. Zhu, Appl. Phys. Lett. **80**, 941 (2002).

[40] L. Brus, J. Phys. Chem. **90**, 2555 (1986).

[41] R. Swanepoel, J. Phys. E: Sci. Instrum. 16, 1214 (1983).

[42] Z. Wang, U. Helmersson, P. O. Kall, Thin Solid Films **405**, 50 (2002).

[43] B. E. Yoldas, P. W. Partlow, Thin Solid Film **129**, 1 (1985).

[44] L. Martinu, D. Poitras, J. Vac. Sci. Technol. A **18**, 2619 (2000).

[45] S. Mahanty, S. Roy, S. Sen, J. Crystal Growth **261**, 77 (2004).

*Corresponding author: benyamin_yarmand@yahoo.com; byarmand@merc.ac.ir